Journal of Statistical Physics, Vol. 111, Nos. 3/4, May 2003 (© 2003)

A Boolean Delay Equation Model of Colliding Cascades. Part I: Multiple Seismic Regimes

Ilya Zaliapin,[1,4] Vladimir Keilis-Borok,[2] and Michael Ghil[3]

Received October 23, 2001; accepted October 11, 2002

We consider a prominent feature of hierarchical nonlinear ("complex") systems: persistent recurrence of abrupt overall changes, called here "critical transitions." Motivated by the earthquake prediction problem, we formulate a model that uses heuristic constraints taken from the dynamics of seismicity. Our conclusions, though, may apply to hierarchical systems that arise in other areas.We use the Boolean delay equation (BDE) framework to model the dynamics of colliding cascades, in which a direct cascade of loading interacts with an inverse cascade of failures. The elementary interactions of elements in the system are replaced by their integral effect, represented by the delayed switching of an element's state.The present paper is the first of two on the BDE approach to modeling seismicity. Its major results are the following: (i) A model that implements the approach. (ii) Simulating three basic types of seismic regime. (iii) A study of regime switching in a parameter space of the loading and healing rates. The second paper focuses on the earthquake prediction problem.

KEY WORDS: Cellular automata; colliding cascades; delay equations; hierarchical modeling; seismic regimes.

[1] International Institute of Earthquake Prediction Theory and Mathematical Geophysics, Russian Academy of Sciences, Moscow, Russia, and Institute of Geophysics and Planetary Physics, University of California, Los Angeles, 90095-1567; e-mail: zal@ess.ucla.edu

[2] International Institute of Earthquake Prediction Theory and Mathematical Geophysics, Russian Academy of Sciences, Moscow, Russia, and Institute of Geophysics and Planetary Physics and Department of Earth and Space Sciences, University of California, Los Angeles; e-mail: vkb@ess.ucla.edu

[3] Department of Atmospheric Sciences and Institute of Geophysics and Planetary Physics, University of California, Los Angeles, and Département Tere-Atmosphère-Océan and Laboratoire de Météorologie Dynamique, Ecole Normale Supérieure, Paris; e-mail: ghil@atmos.ucla.edu

[4] To whom correspondence should be addressed.

0022-4715/03/0500-0815/0 © 2003 Plenum Publishing Corporation

1. BACKGROUND AND MOTIVATION

1.1. Colliding-Cascade (CC) Model

The CC model[1, 2] synthesizes four phenomena that play an important role in many complex systems: (i) hierarchical structure; (ii) external loading (or driving); (iii) ability of the system's elements to fail (break down) under the load, causing redistribution of the load and strength throughout the system; and (iv) the element's ability to heal.

We use in our model a ternary hierarchical structure, shown in Fig. 1. The load is applied at the top of the hierarchy and transferred downwards, forming a *direct cascade of loading*. Failures are initiated at the lowest level of the hierarchy, and gradually propagate upwards, forming an *inverse cascade of failures*, which is followed by *healing*. The interaction of direct and inverse cascades establishes the dynamics of the system: loading triggers the failures, while failures redistribute and release the load.

In the first version of the CC model[1, 2] elementary interactions between its elements have been simulated by a system of ordinary differential equations (ODEs). This version has reproduced several major features of seismicity, including four types of premonitory seismicity patterns. Premonitory increase of the earthquake correlation range, introduced in ref. 2, was later confirmed by analysis of observations.[3, 4]

The present version of the model takes advantage of the BDE framework developed by M. Ghil and associates.[5–7] This paper is focused on design of the model and on multiple regimes of synthetic seismicity, while the study's second part[8] focuses on the earthquake prediction problem.

The paper proceeds as follows. The remainder of the present section provides some background on BDEs and the model's heuristic constraints. The model is formulated in Section 2 and its multiple seismic regimes are described in Section 3. The physics of what determines the prevalence of one regime or another is outlined in Section 4 and the results are further discussed in Section 5.

1.2. Boolean Delay Equations (BDEs)

BDEs represent a novel modeling language especially tailored for the mathematical formulation of conceptual models of systems that exhibit threshold behavior, multiple feedbacks and distinct time delays.[5, 6] BDEs are *semi-discrete dynamical systems*, where the variables are discrete—typically Boolean, i.e., taking the values 0 ("off") or 1 ("on") only—while time is allowed to be continuous. As such they occupy the previously "missing corner" in the rhomboid of Fig. 2, where dynamical systems are classified

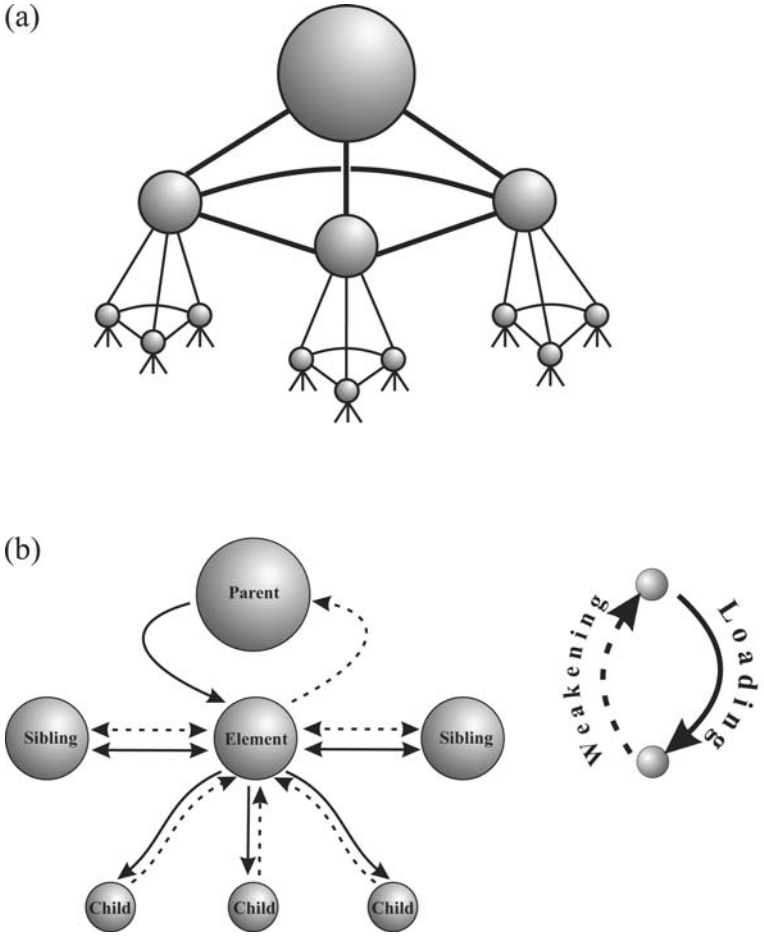

Fig. 1. Structure of the colliding cascade (CC) model with branching number 3. (a) Three highest levels of the hierarchy. (b) Interaction with the nearest neighbors.

according to whether their time (t) and state variables (x) are continuous or discrete.

Systems in which both the variables and time are continuous are called *flows*[9] (upper corner in the rhomboid of Fig. 2). Vector fields, ODEs and partial differential equations (PDEs), functional and delay-differential equations (FDEs and DDEs) and stochastic differential equations (SDEs) belong to this category. Systems with continuous variables and discrete

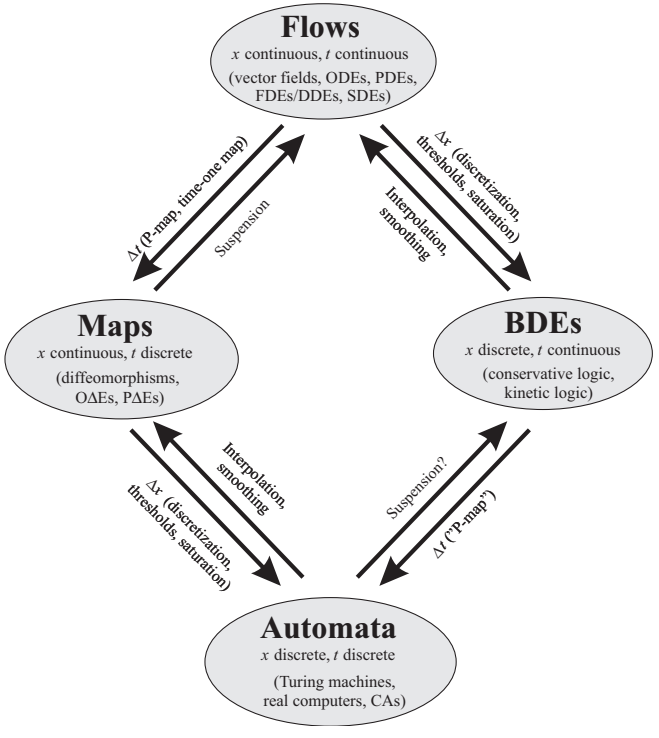

Fig. 2. The place of BDEs within dynamical system theory. Note the links: The discretization of t can be achieved by the Poincaré map (P-map) or a time-one map, leading from **Flows** to **Maps**. The opposite connection is achieved by suspension. To go from **Maps** to **Automata** we use the discretization of x. Interpolating and smoothing can lead in the opposite direction. Similar connections lead from **BDEs** to **Automata** and to **Flows**, respectively. See text for details.

time (middle left corner) are known as *maps*[10] and include diffeomorphisms, as well as ordinary and partial difference equations (O$\triangle$Es and P$\triangle$Es). Automata (lower corner) have both time and variables that are discrete: cellular automata (CAs) and all Turing machines (including real-world computers) are part of this group.[11, 12] BDEs and their predecessors, kinetic and conservative logic, complete the rhomboid in the figure and occupy the remaining middle right corner.

The formulation of BDEs was originally inspired by advances in theoretical biology, following Jacob and Monod's[13] discovery of on-off interactions between genes, which had prompted the formulation of "kinetic logic"[14, 15] and Boolean regulatory networks.[16] The BDE

approach was first applied[17–19] to help interpret paleoclimate records;[20, 21] it was later extended to a broader climate modeling context.[7, 22–24] As the study of complex systems garners increasing attention and is applied to diverse areas—from economics to the evolution of civilizations, passing through physics—related Boolean and other discrete models are being explored more and more.[11, 25, 26]

Our BDE model uses only integer delays. In this sense it is simpler than those previously explored.[5–7] On the other hand, the model studied here has a stochastic component, which has not been studied so far.

1.3. Heuristic Constraints

In its application to seismicity, the model's hierarchical structure represents a fault network, loading imitates the impact of tectonic forces, and failures imitate earthquakes. Heuristic constraints include the major regularities in the observed dynamics of seismicity:[27–30] (i) the seismic cycle; (ii) intermittency in the seismic regime; (iii) the size distribution of earthquakes, usually called the Gutenberg-Richter relation; (iv) clustering of earthquakes in space and time; (v) long-range correlations in earthquake occurrence; and (vi) a variety of seismicity patterns premonitory to a strong earthquake.[27, 30–32] Here we demonstrate that the model-generated seismicity satisfies the first four constraints. The last two are studied in our study's second part.[8]

2. THE MODEL

Lattice models of interacting-element systems are widely applied for modeling seismicity, starting with the pioneering works of Burridge and Knopoff,[33] Allegre *et al.*,[34] Bak *et al.*[35] and Narkunskaya and Shnirman.[36] The theoretical background for such modeling and its results so far are summarized in refs. 29, 31, 32, and 37–42. The predictability of such systems is discussed in refs. 32, 38, and 40. The present study is close in spirit to the modeling described in refs. 34 and 42–48.

In the BDE framework, we replace the detailed interactions between elements by their integral effects. These effects are represented by the delayed switches of an element from one state to another: unloaded vs. loaded and intact vs. failed.

2.1. Outline

(i) The model acts on a ternary graph of depth L (Fig. 1(a)). Each element is a parent of three children that are each other's siblings. An

element is connected to and interacts with its six nearest neighbours: the parent, two siblings, and three children. The top element has neither parent nor siblings; the elements at the lowest level have no children.

(ii) Each element possesses a certain degree of *weakness* or *fatigue*. An element fails when its weakness exceeds a certain threshold.

(iii) The time is discrete: $n = 0, 1, \ldots$. The state of an element e at an epoch n is defined by two Boolean functions, $s_e(n)$ and $l_e(n)$. At each epoch a given element may be either *intact*, $s_e(n) = 0$, or *failed*, $s_e(n) = 1$, and either *unloaded*, $l_e(n) = 0$, or *loaded*, $l_e(n) = 1$.

(iv) An element may switch from one state (s_e, l_e) to another under an impact from its nearest neighbors (Fig. 1(b)).

(v) At the start, $n = 0$, all elements are in the state (0, 0), intact and unloaded. Most of the changes in the state of an element occur in the following cycle:

$$\ldots \to (0, 0) \to (0, 1) \to (1, 1) \to (1, 0) \to (0, 0) \to \ldots$$

(vi) All the interactions take a nonzero time. We model this by introducing four basic time delays: Δ_L, between an element being impacted by the load and switching to the loaded state; Δ_F, between the exceeding the weakness threshold and switching to the failed state; Δ_D, between failure and switching to the unloaded state; and Δ_H, between establishing the healing conditions and switching to the intact (healed) state. In each specific case a delay is determined as described in Sections 2.2 and 2.3 below, depending on the impact of the nearest neighbors of an element.

2.2. Load Switching

The top element of the system is loaded by external forces. The load is transferred down the hierarchy, so that an element on all other levels may receive the load only from its parent and siblings. Each element may transfer the load only to its siblings and children. The load dissipates at the lowest level exclusively. This is reminiscent of 3-D turbulence, where energy enters the system only at the largest scale, is redistributed across all scales, and is finally dissipated at the shortest scales.[49, 50]

The unloaded top element becomes loaded, $(0, 0) \to (0, 1)$, after it remains intact for the time Δ_L. The top element becomes unloaded, $(1, 1) \to (1, 0)$, with the time delay Δ_D after failure.

Load switching for any other element depends on the impact from its neighbors. The total impact $I_e(n)$ on an element e at epoch n is defined by

$$I_e(n) = l_p - l_e + \kappa \sum_i (l_i - l_e). \tag{1}$$

Here the summation is taken over the indices i of the element's siblings, while the index p refers to its parent, and $\kappa \leqslant 1$ is a weighting coefficient.

When the impact I_e becomes nonzero at epoch n, the load is switched after the delay

$$\Delta(n) = [\Delta_L / |I_e(n)|], \tag{2}$$

where $[x]$ is the integer part of x. The type of switching—loading or unloading—is determined by the sign of the impact (1). Load switching does occur even if the impact becomes zero during the delay $\Delta(n)$.

At each epoch n_j, at which the element e, its parent or a sibling switch their load, we define the corresponding epoch $N_e^{(l)}(n_j) = n_j + \Delta(n_j)$ of possible load switching, with $\Delta(n_j)$ given by (2). The load on e actually switches at the earliest one of the epochs $N_e^{(l)}$.

Unloading takes place with the fixed delay Δ_D after a failure.

2.3. Failures and Healing

An element is weakened by the failure of its neighbors. The weakness W_e of element e at epoch n is defined as follows:

$$W_e(n) = cF_c(n) + (1-c)\, F_s(n) + pF_p(n). \tag{3}$$

Here $F_c(n)$ and $F_s(n)$ are the numbers of failed children and siblings of the element e respectively. The Boolean function $F_p(n)$ indicates the weakening that takes place during Δ_D time units after the parent's failure. Note that during this time associated in observations with generation of aftershocks the weakness is transferred down the hierarchy. The coefficients $0 \leqslant c \leqslant 1$, $p \geqslant 0$ determine the impact of a neighbor's failure on e.

An intact element e fails when (i) it is loaded, $l_e(n) = 1$, and (ii) its weakness $W_e(n)$ exceeds a certain threshold W_0. For failure to occur, these conditions have to hold during the time delay

$$\Delta(n) = [\Delta_F \exp(W_0 - W_e(n))]. \tag{4}$$

At each epoch n_j, at which at least one of the element's nearest neighbors switches its state, we determine the corresponding epoch $N_e^{(s)}(n_j) = n_j + \Delta(n_j)$ of state switching, where $\Delta(n_j)$ is given by (4). The actual failure occurs at the earliest one of the epochs $N_e^{(s)}$.

After its failure and subsequent unloading, an element starts to heal. It becomes intact when at least two of its children remain intact for the time Δ_H, independently of the element's load.

2.4. Triggering of Inverse Cascades

In our model, an inverse cascade of failures can only be triggered on the lowest level. For each element on that level we generate the number U_e of its broken children by a random process. The physical rationale is to simulate, in an otherwise deterministic model with a finite (and relatively small) number of levels, the effects of the lower levels in an infinite hierarchy.

Specifically, $U_e(n)$ is defined as a random walk with integer values from 0 to 3; $U_e(0) = 0$. It changes its value at the epochs of a Poisson process with intensity λ. An increment $+1$ or -1 appears if the element is loaded or unloaded, respectively. The value of U_e does not change when $U_e = 0$ and the increment is -1 or when $U_e = 3$ and the increment is $+1$.

While random initial states in BDE modeling were considered in ref. 18 and periodic forcing in ref. 7, the use of random forcing here is new, to the best of our knowledge. It induces model behavior that is statistically stationary or cyclo-stationary, rather than simply periodic.

2.5. Conservation Law and Model Parameters

Our BDE model is dissipative[6] if we associate the loading with an energy influx. The energy dissipates only at the lowest level, where it is transferred out of the model. In any part of the model that does not include its lowest level energy conservation holds, after averaging over sufficiently large time intervals. On small intervals it may not hold due to the discrete time delays involved in energy transfer.

The model has the following parameters: the time delays Δ_L, Δ_D, Δ_F, and Δ_H (Section 2.1); the intensity λ of the initial fracturing (Section 2.4); the dimensionless parameters κ, c and p that determine the neighbors' impact on an element, cf. Eqs. (1)–(3); and the weakness threshold W_0 (Section 2.3). Time is normalized by Δ_F, and the coefficients c and p by W_0, so that $W_0 = 1$. Accordingly, the model has seven independent parameters: Δ_L, Δ_D, Δ_H, λ, κ, c, and p. We kept the last three parameters fixed (see Table I), as well as the ratio $\Delta_H/\Delta_D = 2$, and concentrated on how changes in Δ_L, Δ_H, and λ affect the model's behavior.

2.6. Earthquake Sequence

A model earthquake is the failure of a system's element. The sequence of synthetic earthquakes is represented by a catalog, similar to those produced for the observed earthquakes:

$$\mathbf{C} = \{(t_k, m_k, h_k) : k = 1, 2, \ldots, K; t_k \leqslant t_{k+1}\}; \tag{5}$$

Table I. Fixed Values of the Model's Parameters or Their Range of Variation

	λ	Δ_L	Δ_H	Δ_D	Δ_F	κ	c	p	L
From	10^{-7}	1	1	$\Delta_H/2$	10^3	1/3	2/3	3	6
To	10^{-2}	10^6	10^6						

here t_k is the time of failure; m_k is the level of the broken element counted from the bottom of the hierarchy; and h_k is the position of an element within the model ternary structure (see Fig. 1(a)).

3. MULTIPLE SEISMIC REGIMES

A long-term pattern of seismicity within a given region is usually called a *seismic regime*. It is characterized by the frequency and the irregularity of the strong earthquakes' occurrence; the size distribution of earthquakes; the variability of this distribution with time; and the largest magnitude recorded during a few decades.

In the Earth, one seismic regime may switch to another in the same region;[51, 52] the range of possible regimes is determined by the region's neotectonics. An essential characteristic of a seismic regime is its sequence of *seismic cycles*. Each cycle consists of three consecutive phases:[28] "preseismic" rise of activity that culminates in one or several major earthquakes; "postseismic," gradual decline of activity; and relatively low activity that eventually returns to another rise. Such cycles take place on different time and space scales. The time intervals between consecutive major earthquakes, timing of a particular phase within each cycle, and the maximal magnitude vary strongly from cycle to cycle.

3.1. Regime Description

We simulated a number of earthquake sequences, each spanning the time interval $I = [0, 2 \cdot 10^6]$; the values of the parameters were varied from one simulation to another, as shown in Table I. The synthetic sequences can be divided into three seismic regimes, illustrated in Fig. 3.

Regime H: *High and nearly periodic seismicity* (top panel). The fractures within each cycle reach the top level, $m = L$, with $L = 6$. The sequence is approximately periodic, in the statistical sense of cyclo-stationarity.[53]

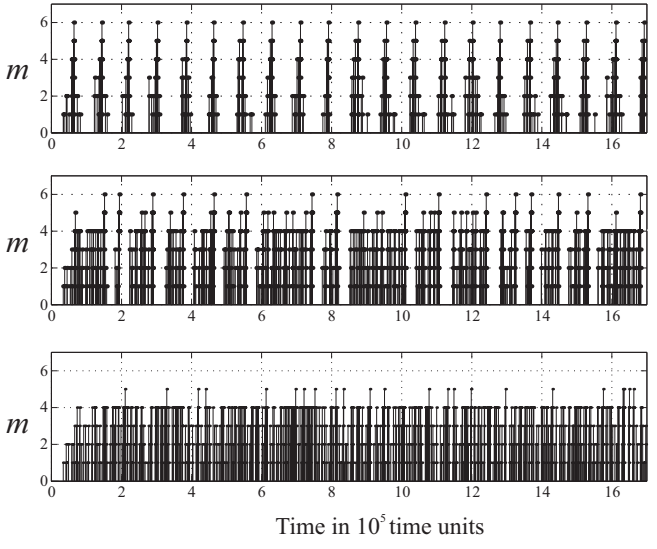

Fig. 3. Three seismic regimes: sample of earthquake sequences. Top panel—regime H, $\Delta_H = 0.5 \cdot 10^4$; middle panel—regime I, $\Delta_H = 10^3$; bottom panel—regime L, $\Delta_H = 0.5 \cdot 10^3$. The rest of the model parameters are fixed: $\Delta_L = 0.5 \cdot 10^4$, $\Delta_F = 10^3$, $\lambda = 0.2 \cdot 10^{-4}$, $\kappa = 1/3$, $c = 2/3$, and $p = 3$.

Regime I: *Intermittent seismicity* (middle panel). The seismicity reaches the top level for some but not all cycles.

Regime L: *Medium or low seismicity* (lower panel). No cycle reaches the top level and seismic activity is much more constant at a low or medium level, without the long quiescent intervals present in Regimes H and I.

3.1.1. Density of Failed Elements

To depict the difference between the regimes described above we show in Fig. 4 the average density $\rho(n)$ of the elements that are in a failed state at epoch n:

$$\rho(n) = [v_1(n) + \cdots + v_m(n)]/L. \tag{6}$$

Here $v_i(n)$ is the fraction of failed elements at the ith level of the hierarchy at the epoch n, L is the depth of the tree. The panels correspond to the three synthetic sequences shown in Fig. 3. The density ρ exhibits the transition from near-periodicity (panel a) to intermittent (panel b) and eventually to low-level noisy behavior (panel c) that appears in Fig. 3.

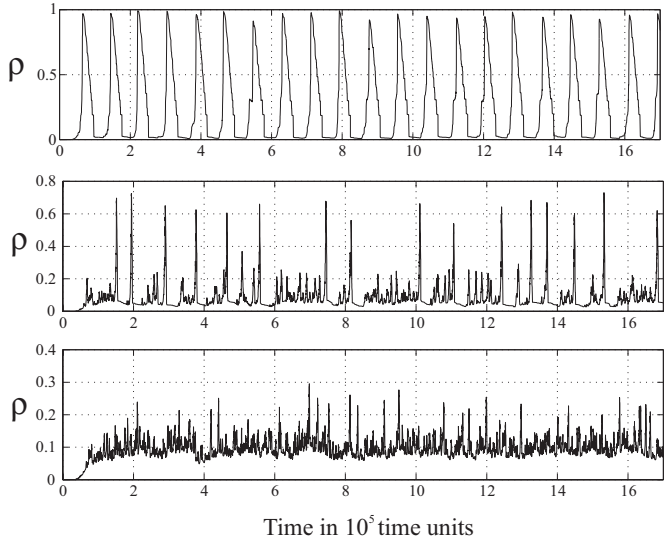

Fig. 4. Three seismic regimes: internal dynamics of the system. The panels show the density $\rho(n)$ of broken elements in the system, as defined by Eq. (6); they correspond to the synthetic sequences shown in Fig. 3. Top panel—Regime H; middle panel—Regime I; and bottom panel—regime L.

3.1.2. Gutenberg-Richter (GR) Relation

Figure 5 displays the magnitude distribution, otherwise known as GR relation, of model earthquakes for the three sequences shown in Fig. 3; it plots the number $N = N(m)$ of earthquakes with magnitude m.

Most frequently mentioned in the literature is the linear form of the GR relation, $\log N(m) = a - bm$. This form corresponds to a power law for the released energy distribution and is attributed to scale invariance of the underlying processes.[29, 50, 54–57] Both in real and modeled seismicity the linear relation is a crude approximation, valid only after considerable averaging in space in time, and in a limited magnitude range.

In our model, the GR relation is quite distinct from one regime to another. For regime H (panel a), the relation is almost perfectly linear over all possible magnitudes, with $b = 0.48$. For regimes I and L (panels b and c, respectively), the GR relation is increasingly convex and thus cannot be characterized well by a single slope b. A straight line with the slope $b = 0.48$ is shown in panels (b) and (c) for comparison. For regime H, the GR relation is stationary, while for the other two it is changing in time (not shown). Figure 5 illustrates deviation from scale invariance—the most important feature of non-linear systems with multilevel hierarchy. In regime H the whole system is periodically crashed (cf. Fig. 4a) which leads

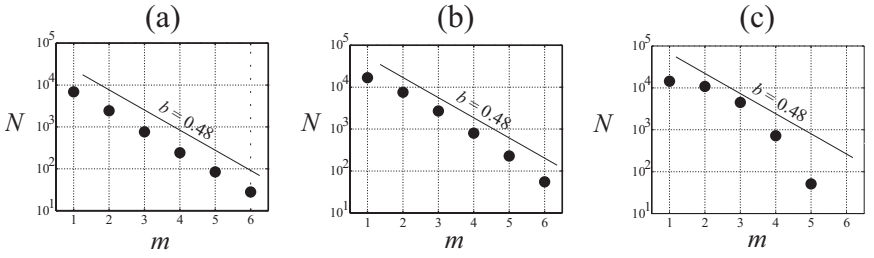

Fig. 5. Three seismic regimes: magnitude distributions (Gutenberg-Richter relation). The distributions are computed for the sequences shown in Fig. 3, over the whole time interval $[0, 2 \cdot 10^6]$ over which the synthetic sequences were generated: (a) Regime H; (b) Regime I; and (c) Regime L. A straight line $N(m) = a - bm$, with $b = 0.48$, is shown in each panel for comparison with Regime H that fits well this approximation.

to the linear GR relation with slope determined by the model's ternary structure. In regimes I and L at each particular epoch a part of the system remains intact. The cascade of fracturing does not always reach the top level and this leads to the downward bend of GR relation at large magnitudes. The failure of the top element is not followed by the crash of the whole system (cf. Fig. 4b, c) and this leads to the downward bend at small magnitudes.

3.2. Regime Diagram

The location of the regimes in the plane of the two key parameters (Δ_L, Δ_H) is shown in Fig. 6. The range of Δ_L and Δ_H values is shown in the figure, while the rest of the parameters are fixed at the values given in the caption to Fig. 3.

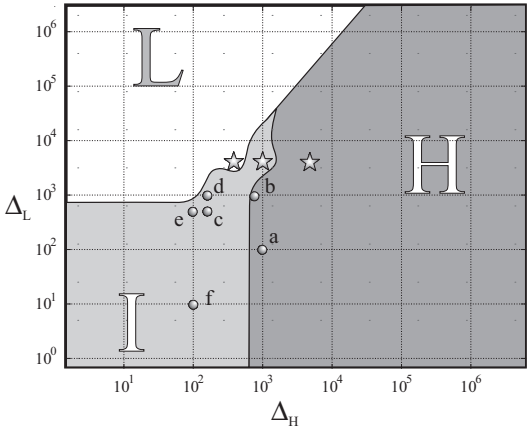

Fig. 6. Regime diagram in the (Δ_L, Δ_H) plane of the loading and healing delays. Stars correspond to the sequences shown in Fig. 3. The points (a)–(f) correspond to the sequences shown in Fig. 10.

Regime H occurs predominantly for high values of Δ_H, that is for low healing rates. Regime L occurs for low Δ_H and high Δ_L, i.e., for high healing rates and very slow loading. Regime I occurs for low Δ_H and low Δ_L, when both the healing and loading rates are high. Its domain also extends toward the upper right edge of the figure and fades away as it approaches the *triple point* at which all three regimes meet.

The three sequences shown in Fig. 3 correspond to the three stars in Fig. 6 at fixed $\Delta_L = 0.5 \cdot 10^4$ and decreasing Δ_H. Next, we analyze what happens to the system when it is driven across regime boundaries.

3.2.1. Irregularity of Energy Release

One of the major differences between regimes resides in the temporal irregularity of seismic energy release. We define here a measure G of that irregularity; this measure will be then used to better illustrate the transitions between regimes in parameter space.

(i) First, define a measure $\Sigma(I)$ of seismic activity within the time interval I as

$$\Sigma(I) = \frac{1}{n} \sum_{i=1}^{n} 10^{Bm_i}, \qquad B = \log_{10} 3. \tag{7}$$

The summation in (7) is taken over all events, labeled by i, within the time interval I; m_i is the magnitude of the ith event. The value of B equalizes, on average, the contribution of earthquakes with different magnitudes, that is from different levels of the hierarchy. In observed seismicity, $\Sigma(I)$ has a transparent physical meaning: given an appropriate choice of B, it estimates the total area of the faults unlocked by the earthquakes during I.[58] This measure is successfully used in several earthquake prediction algorithms.[31]

(ii) Consider a subdivision of the interval I into a set of nonoverlapping intervals of equal length $\epsilon > 0$. For simplicity we choose ϵ such that $|I| = \epsilon N_I$, where $|\cdot|$ denotes the length of an interval and N_I is an integer. Therefore, we have the following representation:

$$I = \bigcup_{j=1}^{N_I} I_j, \quad |I_k| = \epsilon, \quad k = 1,\ldots, N_I, \quad I_j \cap I_j = \varnothing, \quad j \neq k. \tag{8}$$

(iii) For each $n = 1,\ldots, N_I$ we choose an n-subset $\Omega(n) = \{\bigcup_{k=1}^{n} I_{i_k}\}$ that maximizes the value of the accumulated Σ:

$$\Sigma(\Omega(n)) \equiv \Sigma^*(n) = \max_{(i_1,\ldots, i_n)} \left\{ \Sigma \left(\bigcup_k I_{i_k} \right) \right\}, \tag{9}$$

where the maximum is taken over all n-subsets of the covering set (8).

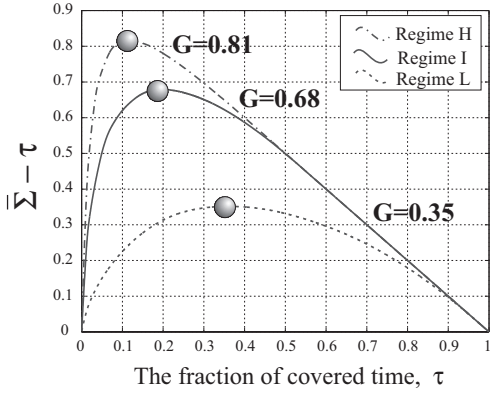

Fig. 7. Measure $G(I)$ of seismic clustering; see Eq. (11). The three curves correspond to the three synthetic sequences shown in Fig. 3.

(iv) Introducing the notations

$$\bar{\Sigma}(n) = \Sigma^*(n)/\Sigma(I), \qquad \tau(n) = n\epsilon/|I|, \tag{10}$$

we finally define the measure of clustering within the interval I as

$$G(I) = \max_{n=1,\ldots,N_I} \{\bar{\Sigma}(n) - \tau(n)\}. \tag{11}$$

Figure 7 illustrates this definition by displaying the curves $\bar{\Sigma} - \tau$ vs. τ for the three synthetic sequences shown in Fig. 3; the maximum of each curve equals the corresponding value of G. The more clustered the sequence, the more convex is the corresponding curve, and the larger the corresponding value of G. For appropriate ϵ, a marked Poisson process with independent marks has $\bar{\Sigma} \equiv \tau$, and thus $G = 0$, which depicts the absence of clustering.

3.2.2. Regime Transitions

Figure 8 illustrates the transition between regimes in the parameter plane (Δ_L, Δ_H). Panel (a) shows a rectangular trajectory in this plane that passes through all three regimes and touches the triple point. We single out 30 points along this trajectory; they are indicated by small circles in the figure. The three pairs of points that correspond to the transitions between regimes are distinguished by larger circles and marked in addition by

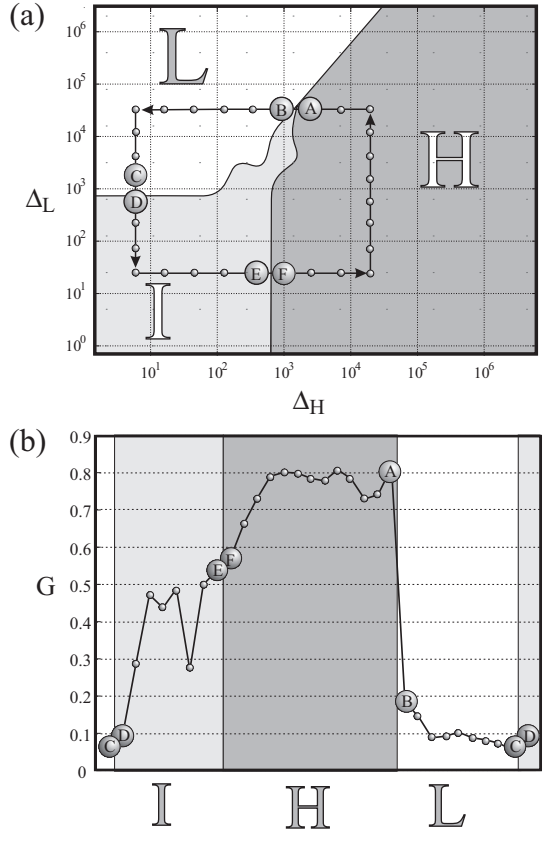

Fig. 8. Bifurcation diagram. (a) Closed trajectory in the parameter plane of Fig. 6; (b) the measure G of clustering illustrated in Fig. 7, calculated along the parameter-plane trajectory shown in panel (a). The transition between points (A) and (B), i.e., between regimes H and L, is quite sharp. See details in the text.

letters, for example (A) and (B) mark the transition from Regime H to Regime L.

We estimate the clustering $G(I)$, with $I = [0, 2 \cdot 10^6]$, for the synthetic sequences that correspond to the 30 marked points along the trajectory in Figs. 8(a) and 8(b) shows the corresponding values of G. These values drop dramaticaly, from 0.8 to 0.18, between points (A) and (B): this means that the energy release switches from highly irregular to almost uniform between Regimes H and L.

The transitions between the other pairs of regimes are much smoother. The clustering drops further, from $G = 0.18$ to $G \approx 0.1$, and then remains at the latter low level within Regime L. It increases gradually, albeit not monotonically, from 0.1 to 0.8 between points (C) and (A), on its way through regimes I and H. The increase of Δ_L along the right side of the rectangular trajectory corresponds to a fixed level of clustering, $G \approx 0.8$.

The transition between regimes is illustrated further in Fig. 9. Each panel shows a fragment of the six synthetic sequences that correspond to the points (A)–(F) in Fig. 8(a). The sharp difference in the character of the energy release at the transition between Regimes H (point (A)) and L (point (B)) is clear. The other two transitions, from (C) to (D) and (E) to (F), are much smoother. Still, they highlight the intermittent character of Regime I, to which points (D) and (E) belong.

3.3. Intermittent Regime

We illustrate here in greater detail Regime I. Figure 10 shows the density of failures $\rho(n)$, cf. Eq. (6), for six synthetic sequences that correspond to points (a)–(f) in the plane (Δ_L, Δ_H) of Fig. 6. The rest of the parameters are fixed at the values given in the caption. The first two sequences, (a) and (b), are taken from Regime H; the other four, (c)–(f), are from Regime I.

The discussion in this subsection is based, in addition to Fig. 10, on certain details of the actual catalog, which is not shown; its relation to the density $\rho(n)$ was illustrated by comparing Figs. 3 and 4 above. The sequence in panel (a) consists of nearly periodic cycles, all of which end with an event of magnitude $m = 6$. The cycles in panel (b) are less regularly spaced and vary somewhat in shape, since this sequence lies in the near vicinity of the boundary between regimes H and I (see Fig. 6).

Panel (c) shows well-developed intermittency. Three types of behavior are present: (i) nearly periodic cycles that end with events of magnitude $m = 6$ and exhibit very little intercycle activity (see for instance the time interval $4.8 \cdot 10^5 \leqslant t \leqslant 5.0 \cdot 10^5$); (ii) nearly periodic cycles that end with events of lower magnitudes and are separated by varying intercycle intervals (e.g., $4.3 \cdot 10^5 \leqslant t \leqslant 4.8 \cdot 10^5$); and (iii) cycles that always end with events of magnitude $m = 6$ but display very strong intercycle activity of variable duration (e.g., $3.5 \cdot 10^5 \leqslant t \leqslant 4.0 \cdot 10^5$). The timing and duration of these three types of behavior vary randomly with time.

Panel (d) illustrates a case when cycles culminating by a strong earthquake with $m = 6$ occur only very rarely. Most of the cycles end with lower magnitudes. This is due to the fact that we approach the domain of Regime L. Panel (e) represents a sequence with very long intervals of nearly

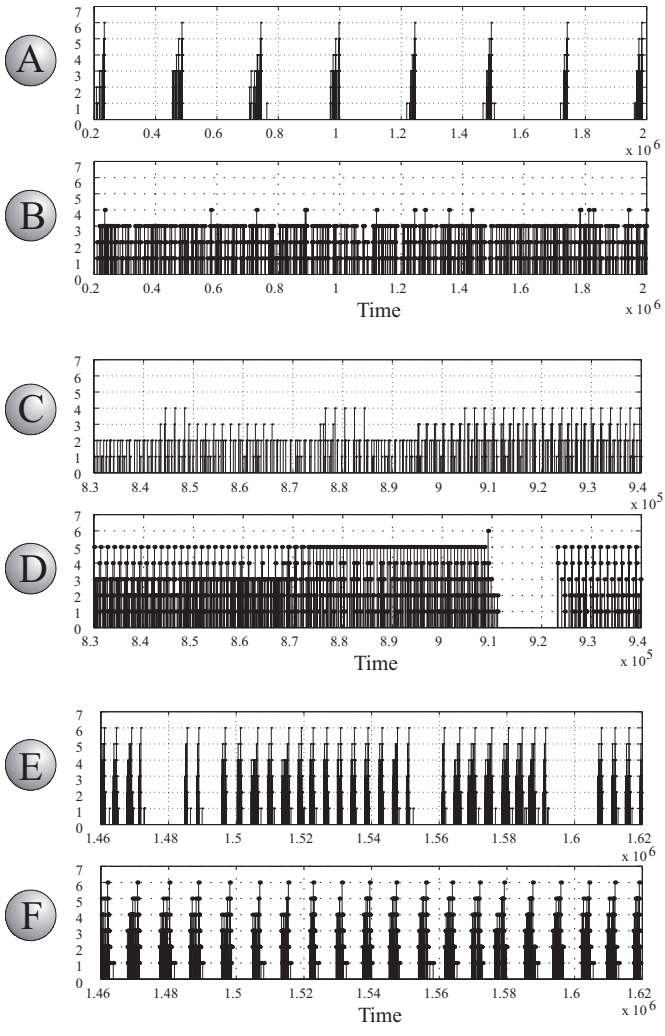

Fig. 9. Synthetic sequences corresponding to the points along the trajectory in parameter space (Fig. 8a.) The panels illustrate the transitions between the regimes H and L—panels (A) and (B); L and I—(C) and (D); and I and H—(E) and (F). The transition from (A) to (B) is very pronounced, while the other two transitions are smoother.

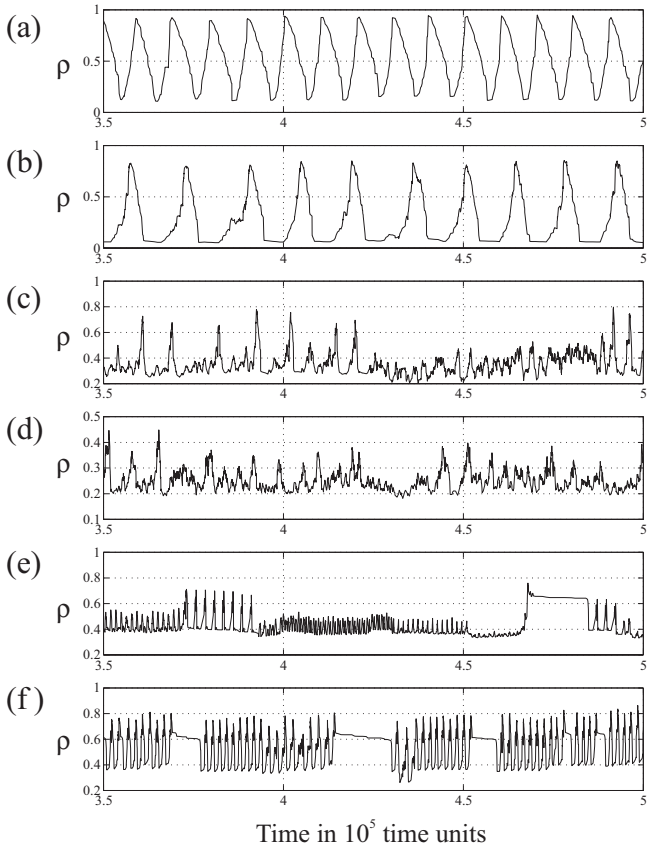

Fig. 10. Different types of intermittent behavior. Each panel shows the density of fractured elements $\rho(n)$ for the corresponding synthetic sequences, over the time interval $[3.5 \cdot 10^5 \;\; 5 \cdot 10^5]$. Differerent panels correspond to different values of the parameters Δ_L and Δ_H, as indicated in Fig. 6, while the rest of the parameters are fixed: $c = 2/3$, $p = 3$, $\kappa = 1/3$, $\lambda = 0.2 \cdot 10^{-4}$, $\Delta_F = 10^3$; (a) $\Delta_L = 10^2$, $\Delta_H = 10^3$; (b) $\Delta_L = 10^3$, $\Delta_H = 7 \cdot 10^2$; (c) $\Delta_L = 5 \cdot 10^2$, $\Delta_H = 2 \cdot 10^2$; (d) $\Delta_L = 10^3$, $\Delta_H = 2 \cdot 10^2$; (e) $\Delta_L = 5 \cdot 10^2$, $\Delta_H = 10^2$; and (f) $\Delta_L = 10$, $\Delta_H = 10^2$.

periodic cycles that differ in mean period and end with different magnitudes. Note that the three sequences shown in panels (c), (d) and (e) are close neighbors in parameter space (see Fig. 6). Nevertheless, they demonstrate a rich variety of long-term seismicity outlooks. This is always the case near a triple point, where any physical system is very sensitive to small changes in parameter values.

Panel (f) shows one of the most interesting situations. All cycles are periodic and end with events of magnitude $m = 6$. But the length of the cycles themselves, as well as that of intercycle intervals, are quite irregular.

4. PHYSICS OF REGIME SWITCHING

We discuss qualitatively in this section the mechanisms that determine the realization of a particular seismic regime in the present model.

4.1. The Role of Memory

Memory effects play a key role in determining the occurrence of one regime or another. These effects can be measured by the decrease of the correlation between the states $(\mathbf{s}, \mathbf{l})$ of the system at epochs $n-k$ and n. If this correlation decays significantly over time intervals of a length k that is comparable with the characteristic duration of a seismic cycle, we speak about short memory. If the correlation decays over times much longer that this duration, we speak about long memory. Long memory leads to the realization of the intermittent regime I. Short memory leads to one of the regimes H or L, depending on loading and healing rates.

4.2. Dependence on Parameters

The model's effective memory, and therefore the resulting regime, is determined by the interplay of parameters. Generally, the changes in the system become faster, and memory shorter, when the initial-fracturing parameter λ (see Section 2.4) increases—so the inverse cascades become more intense—and when either one of the four time delays in Table I decreases. This situation will favor, therefore, the appearance of regimes H or L.

On the other hand, the relative magnitude of the different delays is crucial. For instance, the relation $\Delta_D + \Delta_H \gg \Delta_L$ means that the minimal healing delay is much larger than the loading delay; this favors the realization of Regime H. The opposite relation, $\Delta_D + \Delta_H \ll \Delta_L$, leads to a decrease of the maximal magnitude of earthquakes possible, and hence to the realization of Regime L.

4.3. Healing and Loading

Healing and loading clearly play an important role in the formation of seismic regimes. Seismic activity increases with the loading rate, which is inversely proportional to Δ_L.

Without healing ($\Delta_H = \infty$) the whole system fails in finite time and does not recover at all, as it happens in the case of the fiber-bundle model.[59] When healing is present but slow, $\Delta_H \gg 1$, the system can recover between consecutive total failures and thus give rise to seismic cycles, albeit very long ones. Finally, with fast healing, low-level failures heal so quickly that they can't merge to generate the larger ones. As a result, the inverse cascade never reaches the top level.

The role of each single parameter in establishing a regime is therewith transparent. Note, however, that the realization of a seismic sequence depends on the interplay of parameters: no single parameter alone controls the behavior of the system.

5. DISCUSSION

Our analyses demonstrate that the BDEs framework may serve as the "missing link" for understanding how the elementary interactions within the system determine its global behavior. The BDE model of colliding cascades reproduces the broad spectrum of observed seismic regimes, including their intermittency. Our results provide a basis for the study of the next problem: predicting regime switches. The memory of the system may be a useful control parameter in solving this problem.

Regime switching is well known and intensively studied in climate dynamics;[60–64] similar phenomena arise in percolation theory,[65] as well as in its application to forest fire models.[66] The existence of an infinite percolation cluster is analogous to rupture of the top element in the system considered here. In that way, regime switching could be akin to phase transitions studied in statistical physics. A meaningful connection, if any, is yet to be established, however.

Our regimes H, I and L are dynamical counterparts of the three regimes found analytically by Blanter and Shnirman[48] in a static hierarchical model of defect development that had only an inverse cascade of fracturing. The results presented here are a natural extension of their analytic ones to the more realistic case of colliding cascades of loading and failures.

ACKNOWLEDGMENTS

It is a pleasure to acknowledge numerous discussions with many colleagues. The work of I.Z. and V.K.-B. was supported by The 21st Century Collaborative Activity Award for Studying Complex Systems from the James S. McDonnell foundation. M.G.'s work was supported by NSF Grant ATM-0082131.

REFERENCES

1. A. Gabrielov, V. Keilis-Borok, I. Zaliapin, and W. I. Newman, Critical transitions in colliding cascades, *Phys. Rev. E* **62**:237–249 (2000).
2. A. M. Gabrielov, V. I. Keilis-Borok, I. V. Zaliapin, and W. I. Newman, Colliding cascades model for earthquake prediction, *Geophys. J. Intl.* **143**:427–437 (2000).
3. P. Shebalin, I. Zaliapin, and V. Keilis-Borok, Premonitory raise of the earthquakes' correlation range: Lesser Antilles, *Phys. Earth Planet. Int.* **122**:241–249 (2000).
4. I. Zaliapin, V. I. Keilis-Borok, and G. Axen, Premonitory spreading of seismicity over the fault network in Southern California: Precursor Accord, *J. Geophys. Res.* **107**:2221 (2002).
5. D. Dee and M. Ghil, Boolean difference equations. I: Formulation and dynamic behavior, *SIAM J. Appl. Math.* **44**:111–126 (1984).
6. M. Ghil and A. P. Mullhaupt, Boolean delay equations. II: Periodic and aperiodic solutions, *J. Statist. Phys.* **41**:125–173 (1985).
7. A. Saunders and M. Ghil, A Boolean delay equation model of ENSO variability, *Phys. D* **160**:54–78 (2001).
8. I. Zaliapin, V. Keilis-Borok, and M. Ghil, A Boolean delay equation model of colliding cascades. Part II: Prediction of critical transitions, *J. Statist. Phys.* **111**:839–861 (2003).
9. V. I. Arnol'd, *Geometrical Methods in the Theory of Ordinary Differential Equations* (Springer-Verlag, New York, 1983), p. 334.
10. P. Collet and J.-P. Eckmann, *Iterated Maps on the Interval as Dynamical Systems* (Birkhäuser Verlag, Basel/Boston, 1980).
11. S. Wolfram, *Cellular Automata and Complexity: Collected Papers* (Addison–Wesley, Reading, Mass., 1994).
12. H. Gutowitz, *Cellular Automata: Theory and Experiment* (MIT Press, Cambridge, MA, 1991).
13. F. Jacob and J. Monod, Genetic regulatory mechanisms in the synthesis of proteins, *J. Mol. Biol.* **3**:318–356 (1961).
14. R. Thomas, *Kinetic Logic: A Boolean Approach to the Analysis of Complex Regulatory Systems* (Springer-Verlag, Berlin/New York, 1979).
15. C. Nicolis, Boolean approach to climate dynamics, *Q. J. Roy. Meteor. Soc.* **108**:707–715 (1982).
16. S. A. Kauffman, Metabolic stability and epigenesis in randomly constructed genetic nets, *J. Theor. Biol.* **22**:437–467 (1969).
17. M. Ghil, A. Mullhaupt, and P. Pestiaux, Deep water formation and Quaternary glaciations, *Clim. Dynam.* **2**:1–10 (1987).
18. D. G. Wright, T. F. Stocker, and L. A. Mysak, A note on Quaternary climate modelling using Boolean delay equations, *Clim. Dynam.* **4**:263–267 (1990).
19. L. A. Mysak, D. K. Manak, and R. F. Marsden, Sea-ice anomalies observed in the Greenland and Labrador Seas during 1901–1984 and their relation to an interdecadal Arctic climate cycle, *Clim. Dynam.* **5**:111–133 (1990).
20. C. Emiliani and J. Geiss, On glaciations and their causes, *Geol. Rundschau* **46**:576–601 (1957).
21. W. S. Broecker, D. M. Peteet, and D. Rind, Does the ocean-atmosphere system have more than one stable mode of operation? *Nature* **315**:21–25 (1985).
22. M. S. Darby and L. A. Mysak, A Boolean delay equation model of an interdecadal Arctic climate cycle, *Clim. Dynam.* **8**:241–246 (1993).
23. M. Ghil, Cryothermodynamics: The chaotic dynamics of paleoclimate, *Phys. D* **77**:130–159 (1994).

24. M. Ghil and A. W. Robertson, *Solving Problems with GCMs: General Circulation Models and Their Role in the Climate Modeling Hierarchy. General Circulation Model Development: Past, Present and Future*, D. Randall, ed. (Academic Press, San Diego, 2000), pp. 285–325.
25. G. A. Cowan, D. Pines, and D. Melzer, eds., *Complexity: Metaphors, Models and Reality* (Addison–Wesley, Reading, Mass., 1994).
26. S. A. Kauffman, *At Home in the Universe: The Search for Laws of Self-Organization and Complexity* (Oxford University Press, New York, 1995).
27. V. I. Keilis-Borok, Intermediate-term earthquake prediction, *Proc. Natl. Acad. Sci. USA* **93**:3748–3755 (1996).
28. C. H. Scholz, *The Mechanics of Earthquakes and Faulting* (Cambridge University Press, Cambridge, 1990).
29. D. L. Turcotte, *Fractals and Chaos in Geology and Geophysics*, 2nd ed. (Cambridge University Press, Cambridge, 1997).
30. S. C. Jaume and L. R. Sykes, Evolving towards a critical point: A review of accelerating seismic moment/energy release prior to large and great earthquakes, *Pure Appl. Geophys.* **155**:279–306 (1999).
31. V. Keilis-Borok, Earthquake prediction: State-of-the-art and emerging possibilities, *Annu. Rev. Earth Planet. Sci.* **30**:1–33 (2002).
32. V. I. Keilis-Borok and P. N. Shebalin, eds., Dynamics of lithosphere and earthquake prediction, *Phys. Earth Planet. Int.* **111**:179–330 (1999).
33. R. Burridge and L. Knopoff, Model and theoretical seismicity, *Bull. Seism. Soc. Am.* **57**:341–371 (1967).
34. C. J. Allegre, J. L. Le Mouel, and A. Provost, Scaling rules in rock fracture and possible implications for earthquake prediction, *Nature* **297**:47–49 (1982).
35. P. Bak, C. Tang, and K. Wiesenfeld, Self-organized criticality, *Phys. Rev. A* **38**:364–374 (1988).
36. G. S. Narkunskaya and M. G. Shnirman, Hierarchical model of defect development and seismicity, *Phys. Earth. Planet. Inter.* **61**:29–35 (1990).
37. W. I. Newman, A. Gabrielov, and D. L. Turcotte, eds., Nonlinear dynamics and predictability of geophysical phenomena, *Geophys. Monographs*, Ser. 83 (American Geophysical Union, Washington, DC, 1994).
38. J. B. Rundle, D. L. Turcotte, and W. Klein, eds., *Geocomplexity and the Physics of Earthquakes* (American Geophysical Union, Washington, DC, 2000).
39. G. I. Barenblatt, Micromechanics of fracture, in *Theoretical and Applied Mechanics*, E. R. Bodner, J. Singer, A. Solan, and Z. Hashin, eds. (Elsevier, Amsterdam, 1993), pp. 25–52.
40. J. H. Holland, *Hidden Order: How Adaptation Builds Complexity* (Reading, MA, Addison–Wesley, 1995).
41. D. Sornette, Critical phenomena in natural sciences, *Chaos, Fractals, Self-Organization, and Disorder: Concepts and Tools* (Springer-Verlag, Berlin, Heidelberg, 2000), p. 434.
42. B. E. Shaw, J. M. Carlson, and J. S. Langer, Patterns of seismic activity preceding large earhquakes, *J. Geophys. Res.* **97**:479 (1992).
43. K. Dahmen, D. Ertas, and Y. Ben-Zion, Gutenberg-Richter and characteristic earthquake behavior in simple mean-field models of heterogeneous faults, *Phys. Rev. E* **58**:1494–1501 (1998).
44. A. Gabrielov and W. I. Newman, Seismicity modeling and earthquake prediction: A review, in *Nonlinear Dynamics and Predictability of Geophysical Phenomena*, Geophysical Monograph 83, IUGG, Vol. 18, W. I. Newman, A. Gabrielov, and D. L. Turcotte, eds. (American Geophysical Union, Int. Un. Geodesy Geophys., 1994), pp. 7–13.
45. C. J. Allegre and J.-L. Le Mouël, Introduction of scaling techniques in brittle-fracture of rocks, *Phys. Earth Planet. Inter.* **87**:85–93 (1994).

46. C. Narteau, P. Shebalin, M. Holschneider, J.-L. Le Mouël, and C. J. Allegre, Direct simulations of stress redistribution in the scaling organization of fracture tectonics (SOFT) model, *Geophys. J. Int.* **141**:115–135 (2000).
47. E. M. Blanter, C. Narteau, M. G. Shnirman, and J.-L. Le Mouël, Up and down cascade in a dynamo model: spontaneous symmetry breaking, *Phys. Rev. E* **59**:5,112–5,123 (1999).
48. E. M. Blanter and M. G. Shnirman, Simple hierarchical systems: stability, self-organised criticality and catastrophic behaviour, *Phys. Rev. E* **55**:6397–6403 (1997).
49. U. Frisch, *Turbulence: The Legacy of A. N. Kolmogorov* (Cambridge University Press, 1995).
50. G. S. Golitsyn, The place of the Gutenberg-Richter law among other statistical laws of nature, *Vych. Seism.* **32**:138–161 (2001).
51. A. Press and C. Allen, Pattern of seismic release in the southern California region, *J. Geophys. Res.* **100**:6421–6430 (1995).
52. B. Romanowicz, Spatiotemporal patterns in the energy-release of great earthquakes, *Science* **260**:1923–1926 (1993).
53. A. Mertins, *Signal Analysis: Wavelets, Filter Banks, Time-Frequency Transforms and Applications* (Wiley, Chichester, 1999).
54. B. Gutenberg and C. F. Richter, *Seismicity of the Earth and Associated Phenomena* (Princeton University Press, Princeton, 1954).
55. G. M. Molchan and V. M. Podgaetskaya, Parameters of global seismicity, *Comput. Seism.* **6**:44 (1973).
56. D. L. Turcotte, Seismicity and self-organized criticality, *Phys. Earth Planet. Inter.* **111**:275–294 (1999).
57. L. Knopoff, The magnitude distribution of declustered earthquakes in Southern California, *Proc. Natl. Acad. Sci.* **97**:11880–11884 (2000).
58. V. I. Keilis-Borok and L. N. Malinovskaya, One regularity in the occurrence of strong earthquakes, *J. Geophys. Res.* **69**:3019–3024 (1964).
59. W. I. Newman, D. L. Turcotte, and A. Gabrielov, Log-periodic behavior of a hierarchical failure model with applications to precursory seismic activation, *Phys. Rev. E* **52**:4827–4835 (1995).
60. P. Smyth, K. Ide, and M. Ghil, Multiple regimes in Northern Hemisphere height fields via mixture model clustering, *J. Atmos. Sci.* **56**:3704–3723 (1999).
61. A. Robertson and M. Ghil, Large-scale weather regimes and local climate over the Western United States, *J. Climate* **12**:1796–1813 (1999).
62. E. R. Weeks, Y. Tian, J. S. Urbach, K. Ide, H. Swinney, and M. Ghil, Transitions between blocked and zonal flows in a rotating annulus with topography, *Science* **278**:1598–1601 (1997).
63. M. Kimoto and M. Ghil, Multiple flow regimes in the Northern Hemisphere winter. Part II: Sectorial regimes and preferred transitions, *J. Atmos. Sci.* **50**:2645–2673 (1993).
64. M. Ghil and A. W. Robertson, "Waves" vs. "particles" in the atmosphere's phase space: A pathway to long-range forecasting? *Proc. Natl. Acad. Sci.* **99**:2493–2500 (2002).
65. D. Stauffer and A. Aharony, *Introduction to Percolation Theory*, 2nd ed. (Taylor and Francis, London, 1992).
66. B. D. Malamud, G. Morein, and D. L. Turcotte, Forest fires: an example of self-organized critical behavior, *Science* **281**:1840–1842 (1998).